ARTICLE

Itaconic acid production by co-feeding of *Ustilago maydis*: A combined approach of experimental data, design of experiments, and metabolic modeling

Anita L. Ziegler[1] ![ORCID] | Lena Ullmann[2] | Manuel Boßmann[1] | Karla L. Stein[2] | Ulf W. Liebal[2] | Alexander Mitsos[1,3,4] | Lars M. Blank[2]

[1]Aachener Verfahrenstechnik - Process Systems Engineering (AVT.SVT), RWTH Aachen University, Aachen, Germany

[2]Institute of Applied Microbiology (iAMB), Aachen Biology and Biotechnology (ABBt), RWTH Aachen University, Aachen, Germany

[3]JARA-ENERGY, Aachen, Germany

[4]Institute of Energy and Climate Research: Energy Systems Engineering (IEK-10), Forschungszentrum Jü lich GmbH, Jü lich, Germany

Correspondence

Lars M. Blank, Institute of Applied Microbiology (iAMB), Aachen Biology and Biotechnology (ABBt), RWTH Aachen University, Aachen, Germany.
Email: Lars.Blank@rwth-aachen.de

Abstract

Itaconic acid is a platform chemical with a range of applications in polymer synthesis and is also discussed for biofuel production. While produced in industry from glucose or sucrose, co-feeding of glucose and acetate was recently discussed to increase itaconic acid production by the smut fungus *Ustilago maydis*. In this study, we investigate the optimal co-feeding conditions by interlocking experimental and computational methods. Flux balance analysis indicates that acetate improves the itaconic acid yield up to a share of 40% acetate on a carbon molar basis. A design of experiment results in the maximum yield of 0.14 itaconic acid per carbon source from 100 g L^{-1} glucose and 12 g L^{-1} acetate. The yield is improved by around 22% when compared to feeding of glucose as sole carbon source. To further improve the yield, gene deletion targets are discussed that were identified using the metabolic optimization tool OptKnock. The study contributes ideas to reduce land use for biotechnology by incorporating acetate as co-substrate, a C2-carbon source that is potentially derived from carbon dioxide.

KEYWORDS

acetate, design of experiments, itaconic acid, metabolic modeling, strain design, *Ustilago maydis*

1 | INTRODUCTION

The plant pathogen *Ustilago maydis* is a well-established model organism in the field of cell biology, and is in the last decade used in biotechnology due to its natural production of a wide range of value-added molecules (Becker et al., 2023; Kämper et al., 2006; Martínez-Espinoza et al., 2002). The highly versatile product spectrum contains organic acids such as itaconic, malic, and succinic acid, polyols, and extracellular glycolipids. These molecules are considered value-added chemicals with potential applications in the pharmaceutical, food, and chemical industries (Geiser et al., 2014; Hosseinpour Tehrani, Becker, et al., 2019; Saha, 2017). Via metabolic engineering, this broad spectrum was narrowed down specifically to itaconic acid (Becker et al., 2020). Itaconic acid itself is a bio-derived platform

---

Anita L. Ziegler and Lena Ullmann contributed equally to this study.

chemical with uses ranging from polymer synthesis to biofuel production (Steiger et al., 2017).

Currently, industrial itaconic acid production is performed using the filamentous fungus *Aspergillus terreus* (Kuenz & Krull, 2018; Okabe et al., 2009). However, itaconic acid production with *A. terreus* displays a challenging process as its production depends on a filamentous morphology, which is required for its high productivity, leading to an increase in production costs (Becker et al., 2020; Gyamerah, 1995; Karaffa et al., 2015). In contrast, advantages of itaconic acid production using *U. maydis* are its unicellular yeast-like growth, high productivity, yields, and titers with a reduced byproduct spectrum due to metabolic engineering (Hosseinpour Tehrani, Becker et al., 2019, Hosseinpour Tehrani, Saur, et al., 2019, Hosseinpour Tehrani, Tharmasothirajan, et al., 2019). By combining metabolic engineering strategies and an integrated process design, a maximum itaconic acid titer of $220 \, \text{g L}^{-1}$ was achieved, while for the last 70 years, itaconic acid has been produced using *A. terreus*, reaching titers of $130 \, \text{g L}^{-1}$ (Karaffa et al., 2015).

The current biotechnological processes for itaconic acid production with *A. terreus* and *U. maydis* are based on carbohydrates, such as molasses and glucose (Kuenz & Krull, 2018; Ullmann et al., 2021). With the overarching goal of a carbon-neutral itaconic acid production process, Ullmann et al. (2021) investigated the potential to (co-)consume CO_2-derived C2 compounds such as acetate. A recent study published by Romero-Aguilar et al. (2023) demonstrated growth of *U. maydis* on acetate as a sole carbon source. The results indicate that *U. maydis* can grow without a loss of viability in a medium containing acetate as the carbon source, whereas the minimal media contained 1% acetate.

Since *U. maydis* is a model organism, efficient genetic tools are available, such as CRISPR/Cas (Wege et al., 2021), high-quality draft genome sequences as well as annotated genomes (Geiser, Ludwig, et al., 2016; Ullmann et al., 2022). Further, a genome-scale metabolic model (GSMM) for *U. maydis* iUma22 was published by Liebal et al. (2022). Those tools enable the investigation of pathogenic mechanisms, biodiversity within the Ustilaginaceae family and biotechnological applications like the metabolic engineering of secondary metabolite production of *U. maydis*.

With the GSMM as a basis, flux balance analysis (FBA) gives insights into the metabolism of the organism (Orth et al., 2010; Varma & Palsson, 1994). To further enhance the product yield, several bilevel optimization formulations exist to suggest optimal modifications (Apaydin et al., 2017; Burgard et al., 2003; Kim et al., 2011; Ren et al., 2013; Tepper & Shlomi, 2010). By deleting a gene, the reactions corresponding to this gene cannot carry flux anymore and hence, the production of, for example, unwanted side products can be eliminated. The formulation OptKnock by Burgard et al. (2003) is a simple, but powerful algorithm to suggest optimal modifications of the metabolic network.

A recent study by Park et al. (2019) exploited the potential of co-feeding strategies, boosting bioproduct synthesis. Since each substrate has unique efficiencies for carbon, energy and cofactor generation, varying the relative amounts of substrates in the mixture allows fine-tuning of carbon to-energy-to-cofactor ratios Park et al. (2019). CO_2-based substrates such as acetate and formate as carbon sources recently gained interest and show potential for improved itaconic acid production with various Ustilaginaceae. Nevertheless, their utilization remains challenging. Acetate at higher concentrations is toxic, whereas co-utilization with glucose challenges the underlying regulatory network of microbes favoring sugar utilization (Enjalbert et al., 2017; Kretschmer et al., 2018; Roe et al., 1998; Russell & Diez-Gonzalez, 1998).

Herein, we investigate the co-substrate metabolization of acetate by *U. maydis* MB215 focusing on design of experiments (DoE) cultivation experiments concerning growth rate, substrate consumption rates and itaconic acid production. We conduct FBA, resulting in gene knockout predictions via OptKnock identifying three knockouts that could potentially enhance itaconic acid production. Further, we compare experimental results to FBA results to gather further insights into *Ustilago's* metabolism. The DoE experiments resulted in growth and substrate uptake data to improve predictions of the GSMM-based FBA simulations. This study contributes to the goal of a reduced land use for biotechnological production processes. By incorporating CO_2-derived acetate as a co-substrate, the required glucose can be reduced as a more efficient itaconic acid production is demonstrated. Thus, the land used for glucose production can be reduced by incorporating acetate to the process.

2 | METHODS

2.1 | Culture conditions

For the cultivation experiments, *U. maydis* strain MB215 was used. Growth and production experiments were performed using modified Tabuchi medium (MTM) according to Geiser, Przybilla, et al. (2016) containing $0.2 \, \text{g L}^{-1} \, MgSO_4 \cdot 7H_2O$, $0.01 \, \text{g L}^{-1} \, FeSO_4 \cdot 7H_2O$, $0.5 \, \text{g L}^{-1} \, KH_2PO_4$, 1 mL L^{-1} vitamin solution, 1 mL L^{-1} trace element solution, and as buffer $19.5 \, \text{g L}^{-1}$ 2-(N-morpholino) ethanesulfonic acid (MES) or $33 \, \text{g L}^{-1} \, CaCO_3$ (Geiser, Przybilla, et al., 2016). The carbon sources glucose and sodium acetate were used at changing ratios, see text for detail. NH_4Cl was added in indicated concentrations. The vitamin solution contained (per liter) 0.05 g D-biotin, 1 g D-calcium pantothenate, 1 g nicotinic acid, 25 g myo-inositol, 1 g thiamine hydrochloride, 1 g pyridoxol hydrochloride, and 0.2 g para-aminobenzoic acid. The trace element solution contained (per liter) 1.5 g EDTA, 0.45 g $ZnSO_4 \cdot 7H_2O$, 0.10 g $MnCl_2 \cdot 4H_2O$, 0.03 g $CoCl_2 \cdot 6H_2O$, 0.03 g $CuSO_2 \cdot 5H_2O$, 0.04 g $Na_2MoO_4 \cdot 2H_2O$, 0.45 g $CaCl_2 \cdot 2H_2O$, 0.3 g $FeSO_4 \cdot 7H_2O$, 0.10 g H_3BO_2, and 0.01 g KI. Cultivation experiments were performed at 30°C.

The DoE was performed in System Duetz® (24 deep-well microtiter plates, EnzyScreen, Heemstede) with a filling volume of 1.5 mL (1200 rpm, 80% humidity, $d = 50$ mm, Infors HT Multitron Pro shaker) (Duetz et al., 2000). Cultures were inoculated in parallel into multiple microtiter plates to a final OD_{600} of 0.5 with cells from an overnight culture in MTM. Tested media combinations are listed in

Tables A1 and A2. A complete plate was taken as a sacrificial sample for each sample point to ensure continuous oxygenation. Samples for analytical methods were taken at eight time points distributed throughout the experiment. Each harvest time occurred after consecutive 24 h. The respective last two plates were harvested after an additional 48 h. Experiments were terminated latest after 168–240 h when a stable itaconic acid production was observed. Controlled batch cultivations were performed in a BioFlow 120 bioreactor with a total volume of 1.3 L and a working volume of 0.5 L in combination with DASware Control Software 5.3.1. (Eppendorf). During cultivation, pH was monitored via online pH probes (phferm, Hamilton) and maintained at pH 6.5 by automatic addition of 10M NaOH and 1M HCl. Dissolved oxygen tension (DOT) was kept constant at approximately 80% saturation by automatic adjustment of the stirring rate (800–1200 rpm). The bioreactor was aerated with an aeration rate of 1 L min^{-1} (2 vvm), while evaporation was limited by sparging the air through a water bottle. The temperature was set to 30°C. The bioreactor was inoculated to a final OD_{600} of 0.5 with cells from an overnight culture in 50 mL MTM containing 50g L^{-1} glucose and 5 g L^{-1} sodium acetate.

2.2 | Process analytics

Cell growth was determined by measuring the optical density at 600 nm (OD_{600}) with an Ultrospec 10 Cell Density Meter (Amersham Biosciences). Carbon sources and metabolites such as glucose, acetate, itaconate, malate, succinate and erythritol in the supernatant were analyzed via high-performance liquid chromatography (HPLC). All samples were filtered with Rotilabo®syringe filters (CA, 0.20 μm) and were afterward diluted in a range of 1:5–1:50 with 5 mM H_2SO_4. Supernatants were analyzed in a DIONEX UltiMate 3000 HPLC System (Thermo Scientific) with a Metab-AAC column (300 × 7.8 mm column, ISERA). Elution was performed with 5 mM H_2SO_4 at a flow rate of 0.6 mL min^{-1}, and a temperature of 40°C. For detection, a SHODEX RI-101 detector (Showa Denko Europe GmbH) and a DIONEX UltiMate 3000 Variable Wavelength Detector set to 210 nm were used. Analytes were identified via retention time and UV/RI quotient compared to standards. All values are the arithmetic mean of two to four biological replicates. Error bars indicate the standard deviation from the mean. Statistical analysis of significant difference (p-value) was performed using unequal variances t-test with unilateral distribution (*$p < 0.05$).

2.3 | Design of experiments

The software Design Expert 11 (Stat-Ease) was used to set up and evaluate the DoE. A response-surface, three-factor central composite design (CCD) was chosen to simultaneously evaluate the influence of varying concentrations of glucose and sodium acetate on the growth of *U. maydis* MB215 as well as the itaconic acid production. For the DoE predicting the effect of co-feeding glucose and acetate on the

growth rate, nine different conditions were tested. All conditions were performed as fourfold replicates, except the central condition (45 g L^{-1} glucose and 6.25 g L^{-1} acetate) as eightfold replicates (Table A1). The model predicting itaconic acid production during acetate co-metabolization cultivations was set up as stated in the following. Nine different conditions were tested, whereas the approaches with the lowest (26 g L^{-1}) and highest (104 g L^{-1}) glucose concentration, as well as the approaches with the lowest and highest acetate concentration, were carried out as duplicates. All remaining medium-level (30–100 g L^{-1}) glucose conditions were implemented in triplicates, except the central condition (65 g L^{-1} glucose and 7 g L^{-1} sodium acetate), as an octuplet (Table A2). To enhance the significance of the model, each condition was tested in replicates. Factors showing a significant influence ($p < 0.05$) were incorporated into the model. If a factor with a nonsignificant influence was substantial for maintaining the model hierarchy, exceptions were made. The input data were transformed, if necessary, according to the recommendations of the software. To prove the predicted conditions and confirm the design, validation in 24-deep well plates and up-scaling shaking flasks were performed.

2.4 | FBA and genome-scale model

FBA determines the reaction fluxes within an organism when the metabolism is at steady state (Orth et al., 2010; Varma & Palsson, 1994), and is based on the metabolic network. The metabolic network includes all known reactions and metabolites inside the cell, together with the stoichiometric factors of the reactions and information on the enzymes catalyzing the reactions. The reaction fluxes are determined by solving the following optimization problem, a linear program:

$$\max_{\mathbf{v} \in \mathbb{R}^n} \quad \mathbf{c}^T\mathbf{v} \qquad \rightarrow \text{objective function}$$
$$\text{s.t.} \quad \mathbf{Sv} = \mathbf{0} \qquad \rightarrow \text{mass balance constraint}$$
$$\mathbf{v}_{lb} \leq \mathbf{v} \leq \mathbf{v}_{ub} \rightarrow \text{constraints on fluxes,}$$

where $\mathbf{v}$ denotes the flux vector with n entries, $\mathbf{S}$ is the stoichiometric matrix, and $\mathbf{v}_{lb}$ and $\mathbf{v}_{ub}$ are parameter vectors imposing lower and upper bounds on the fluxes, respectively. The objective function represents, for example, the biomass production or the target chemical production, by selecting appropriate values for the cost vector $\mathbf{c}^T$. The mass balance constraint represents mass conservation for each metabolite, assuming steady state.

The FBA computations are based on an updated version (v1.1) of the GSMM of *U. maydis* (Liebal et al., 2022). In model v1.1, the exchange reaction for formate was added, and CO_2 uptake was enabled up to a rate of 10mmol g_{DW}^{-1} h^{-1}. To prevent nonphysical reactions fluxes, in model v1.1, the following reactions were defined as irreversible: acetylphosphate *fructose-6-phosphate phosphoketolase* (E.C. 4.1.2.22), *phosphoketolase* (E.C. 4.1.2.9) and the phosphoenol-pyruvate carboxy kinase related reaction *RXN-12481* (E.C. 4.1.1.32). The activity of following reactions resulted in unrealistic overall flux

distributions and thus, they were deactivated in v1.1: methanol dehydrogenase RXN-11453 (E.C. 1.2.98.4), pseudo-catalase PRDXI (E.C. 1.11.1.6), and ATP-citrate-proline lyase ACITL (E.C. 2.3.3.8). Newly added reactions based on experimental evidence include the mannitol production from mannose-6-P via the pseudo reaction *PseudoMan6P2Mnl* (Schipper, 2009) and cytoplasmic isocitrate lyase activity *ICL*. The updated model is available on the *U. maydis* GSMM Github page as v1.1 (https://github.com/iAMB-RWTH-Aachen/Ustilago_maydis-GEM/tree/v1.1).

For investigating co-feeding conditions, the uptake of glucose and acetate were varied. To keep results comparable, the total flux of carbon atom was kept constant. Glucose has six carbon atoms and acetate has two carbon atoms, and hence, the equation

$$v_C = 6 \cdot v_{Glc} + 2 \cdot v_{Ace}$$

was set as additional constraint. When setting the total carbon flux and varying the acetate flux, the corresponding glucose flux was calculated during FBA. using the software COBRAPy (Ebrahim et al., 2013) and the open source solver GLPK. The code for the FBA computations is openly available (https://github.com/iAMB-RWTH-Aachen/Ustilago_maydis-GEM/tree/master/data/AcetateCofeed).

2.5 | Optimal genetic modifications

Genetic modifications influence the flux through a metabolic network. Deletion of a certain gene inhibits the flux through the reaction associated to this gene. Optimal reaction knockouts were suggested by using the bilevel optimization formulation OptKnock (Burgard et al., 2003):

$$\begin{aligned} &\max_{\mathbf{y} \in \{0,1\}^q} && v_{target} \\ &\text{s.t.} && \max_{\mathbf{v} \in \mathbb{R}^n} && v_{biomass} \\ &&& \text{s.t.} \quad \mathbf{Sv} = 0 \\ &&&\quad (\mathbf{By})_i \cdot v_{lb,i} \leq v_i \leq (\mathbf{By})_i \cdot v_{ub,i} \quad \forall i \in (1, 2, ..., n) \\ &&&\quad \sum_{i=1}^{n} (1 - y_i) \leq K, \end{aligned} \tag{1}$$

where the vector **y** denotes the knockouts, that is, $y_i = 0$ indicates knockout of reaction i. The maximum number of knockouts is described by K. Reversible reactions are transformed into two irreversible reactions. The original number of—possibly reversible— reactions is denoted with q, the number of reactions in the irreversible network is n. The matrix **B** is a matrix that maps the irreversible reactions to their original—possibly reversible—reaction. For creating the irreversible network, the software COBRAtoolbox (Schellenberger et al., 2011) was used. The upper level of the optimization program describes the bioengineering objective to maximize the flux of the target product, whereas the lower level describes the microorganism that aims to maximize the biomass flux. The reformulated form of OptKnock as a single-level program was implemented in the optimization language libALE (Djelassi & Mitsos, 2019)

and solved using libDIPS (Jungen et al., 2023) with gurobi 9.5.2 (Gurobi Optimization, LLC, 2022) as solver. The code for the OptKnock computations is openly available (https://github.com/iAMB-RWTH-Aachen/Ustilago_maydis-GEM/tree/master/data/AcetateCofeed).

3 | RESULTS AND DISCUSSION

With *U. maydis*, itaconic acid is produced in a two-phase process. An initial growth phase is followed by the production phase upon depletion of a growth-limiting nutrient, here, itaconic acid production is induced under nitrogen limitation (Maassen et al., 2014). Thus, the total amount of itaconic acid produced in a process is also dependent on the amount of biomass produced. If the growth-limiting nutrient is provided in a higher concentration, more biomass will be formed. This will likely increase the volumetric productivity, but will also decrease the overall yield, since more carbon source is consumed in the formation of the biomass. The trade-off of yield and rate under co-feeding conditions was further examined by simulations and wet-lab experiments.

3.1 | Exploring the range of co-feeding using FBA

To explore the range of co-feeding, we determined the theoretical growth rate and the theoretical itaconic acid flux up to a relative acetate carbon-flux of 100%. Figure 1 shows the results.

We conducted the FBA with a carbon flux of 13.2 mmol g_{DW}^{-1} h^{-1}, which is equivalent to a glucose uptake rate of 2.2 mmol g_{DW}^{-1} h^{-1} (Liebal et al., 2022) and performed the FBA in steps of 1%. Although the mechanism of acetate stress is not explicitly included in iUma22, a decrease in the growth rate with increasing relative acetate carbon ratio could be reproduced, as visualized in Figure 1a. Moreover, a bendpoint comes visible at a relative acetate C-flux of 35%. Interestingly, for ratios of acetate higher than 35%, there exist several possible solutions for achieving the same optimal growth rate. In the presented solution in Figure 1a, all available carbon is metabolized by the organism. However, other solutions exist where not all available carbon of 13.2 mmol g_{DW}^{-1} h^{-1} is taken up, and, hence, the metabolic configurations can vary. At around 92% acetate in the substrate, the solution becomes infeasible. Presumably, not all metabolites included in the biomass exchange reaction, that is, necessary for biomass production, can be metabolized from acetate.

To explore the range of co-feeding for itaconic acid flux, we determined the maximal theoretical itaconic acid flux. Maximal theoretical flux means that we did not impose a threshold on the flux of biomass. The result of this study is shown in Figure 1b. The maximal theoretical flux of itaconic acid on pure glucose (0% C-mol acetate per C-mol total), is 2.51 mmol g_{DW}^{-1} h^{-1}, with a yield of around 0.95 mol mol^{-1}. Presumably, itaconic acid can only be formed from glucose via losses, for example, via the pyuravte dehydrogenase, which also produces CO_2. The itaconic acid flux rises linearly to a maximum of 2.63 mmol g_{DW}^{-1} h^{-1} (>0.99 mol mol^{-1} yield), with a corresponding increase in the relative carbon acetate
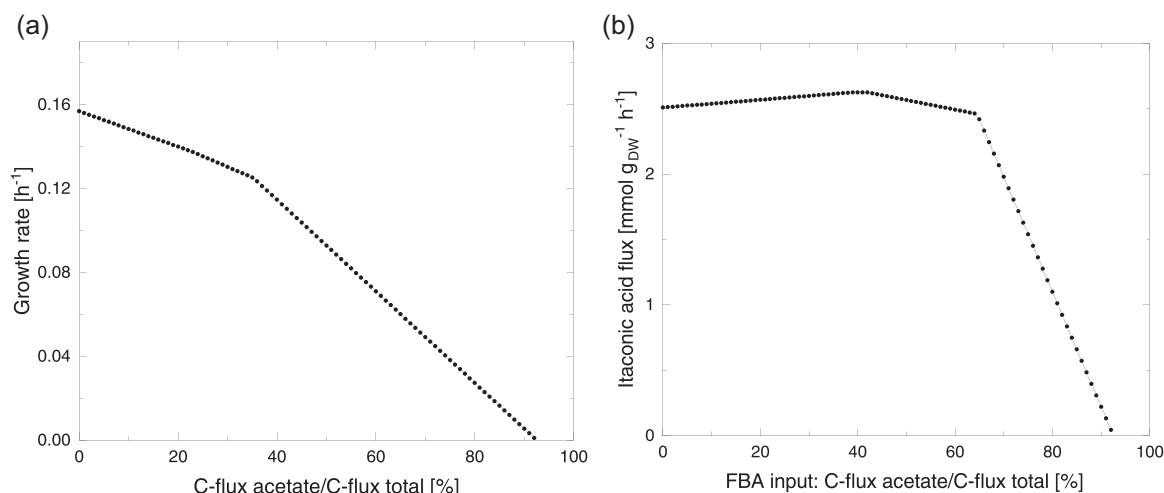
FIGURE 1 Simulated growth rate and itaconic acid flux over the relative acetate carbon uptake (C-flux) predicted by flux balance analysis (FBA) with total and constant C-mol uptake rate of 13.2 mmol g_{DW}^{-1} h^{-1}. The FBA was optimized for growth in (a) and itaconic acid production with no threshold on biomass growth in (b).

uptake ratio to 41%. The maximal theoretical flux is reached on a plateau between 41% and 42% relative carbon flux acetate. Presumably, one or several metabolites needed for itaconic acid production are synthesized better from acetate than from glucose, which is why a certain share of acetate boosts the itaconic acid production. Further increasing the relative acetate carbon uptake ratio reduces the yield to 0.94 mol mol^{-1} (2.46 mmol g_{DW}^{-1} h^{-1} itaconic acid flux) at 64% relative acetate input. The acetate carbon ratio of 64% is a threshold, beyond which the overall carbon uptake rate decreases for both substrates and the flux limits are not necessarily reached. Again, this is due to multiple possible solutions inside the metabolic network that fulfil the maximal itaconic acid flux at the respective condition. It comes visible that beyond a share of 92% carbon flux acetate per carbon flux total, the flux of itaconic acid would become negative, which is not a feasible solution. Presumably, similar to the observations on the simulated growth rate, not all metabolites that are necessary for itaconic acid production, can be metabolized by acetate.

We draw the following conclusions from this study: First, co-feeding of acetate can increase the theoretical flux of itaconic acid in comparison to pure glucose as substrate. Second, the model reproduces the expected growth inhibition on pure acetate. Third, the bend points can indicate that the metabolism switches reaction pathways at these points. Fourth, FBA computations suggest that itaconic acid production on pure acetate is not possible.

To get a better understanding of the flux distributions with varying acetate C-mol ratios in the substrate, the three extreme flux distributions F1 (corresponding to 0% C-mol acetate in the substrate), F2 (40% C-mol acetate), and F3 (60% C-mol acetate) were selected to investigate the metabolic flux details. Figure 2 shows the strategies of carbon conversion to itaconate for different glucose-acetate uptake ratios by depicting relevant pathways with their normalized carbon fluxes.
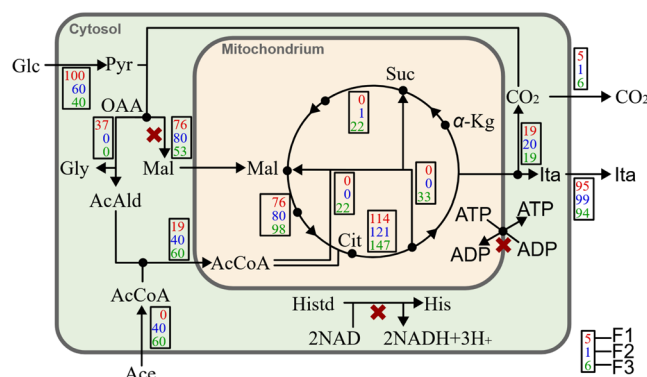

FIGURE 2 Flux distributions of three simulated flux solutions F1, F2, and F3 of Figure 1b for different acetate substrate ratios optimized for itaconic acid production. F1 corresponds to 0%, F2 to 40%, and F3 to 60% C-mol acetate in the substrate mix. For comparability, the carbon uptake was normalized to 100 mmol g_{DW}^{-1} h^{-1} and each reactions shows the conversion rate of participating carbon atoms. The pentose phosphate cycle is inactive, ALD represents a pathway including the Threonine Aldolase reaction (E.C. 4.0.2.5) which was used to convert oxaloacetate via threonine to acetaldehyde. The red crosses indicate mutations with increased itaconic acid and biomass production identified by optimization with the maximum number of knockouts K = 3 (see Equation 1).

The flux values at each reaction represent the percent of converted carbon atoms, relative to the total carbon atom uptake. For example, the ALD-pathway of F1 (red, top number) represents the conversion of 37 oxaloacetate carbon atoms to 18 carbon atoms of glycine (Gly) and 18 carbon atoms of acetaldehyde (AcAld) which are further transformed to acetyl-CoA (AcCoA). The resulting AcCoA relocates into the mitochondria for further reactions in the TCA. The optimal path with highest icaconic acid production (F2, blue) avoids glyoxylate shunt fluxes. While also the glucose only itaconic acid

production route displays inactive glyoxylate shunt (*F1*, red), the AcCoA for the citrate synthase reaction has to be generated from pyruvate. The model chooses a hypothetical route via the threonine aldolase reaction to avoid loosing CO_2 via pyruvate dehydrogenase. The acetate co-feed in scenarios *F2* and *F3* avoid the detour route and results in a more efficient glucose carbon utilization.

3.2 | Improving the itaconic acid yield by knocking out three reactions

Gene knockouts were predicted using OptKnock in a range of one to three knockouts. The carbon input was set to 13.2 mmol g_{DW}^{-1} h^{-1} and a threshold on biomass was induced, which was 0.016 h^{-1}. Without knockouts, no itaconic acid was produced when conducting a FBA with the objective of biomass formation and 0.16 h^{-1} biomass was formed as only glucose was chosen as carbon source by the optimizer. With one to two knockouts, no significant improvement came visible, meaning that no itaconic acid was formed. We conclude that two knockouts are not sufficient to improve the yield of itaconic acid. With three knockouts, OptKnock predicted a significant improvement in the itaconic acid flux, which was 0.53 mmol g_{DW}^{-1} h^{-1}, while decreasing the biomass forma-tion to 0.029 h^{-1}. Hence, more carbon atoms were used in itaconic acid formation and less in biomass formation, which was intended. Figure 2 shows the reactions that were targeted for knockout by red crosses. The predicted reactions are "TRANS Adenine Nucleotide Transporter," "Cytosolic MALATE-DEH-RXN," and "HISTD." The optimizer chose for pure glucose and no acetate as carbon input. When optimizing on glucose from the start, the last reaction of the suggested ones ("HISTD") changed to "PPCOACm." This indicates that there are several reactions that lead to the optimal solution. The results from OptKnock, however, cannot guarantee the improved itaconic acid yield. To tackle this drawback, more advanced formulations (Apaydin et al., 2017; Tepper & Shlomi, 2010) should be considered in future work. Moreover, "Cytosolic MALATE-DEH-RXN" as well as "TRANS Adenine Nucleotide Transporter" are reactions that actively take part in the itaconic acid production, which is why the knockout of these reactions are questionable with biological experience. Formulations that are suitable for a modified organism (Kim et al., 2011; Ren et al., 2013) should therefore be considered next. Moreover, the suggested knockouts should also be tested experimentally, which, however, was out of the scope of this work.

3.3 | Comparing the experimental growth rate with the predicted growth rate under co-feeding conditions

We evaluated the growth rate under nine different co-feeding conditions (Table A1). Thereby, experiments were performed using a DoE approach. In contrast to one-factor-at-a-time (OFAT) optimiza-tion, a DoE approach allows to gain a deeper understanding of how different combinations of the following factors, for example, glucose and sodium acetate, impact growth rate. FBA indicates that acetate
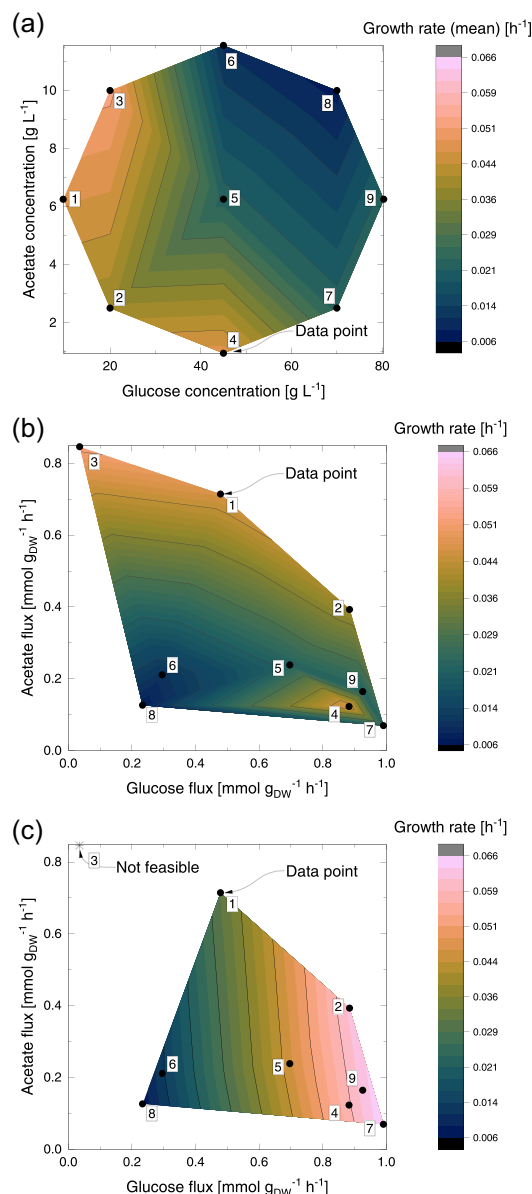

FIGURE 3 Growth rate over glucose and acetate flux. Panel (a) shows experimental data on growth rate over glucose and acetate concentration obtained during the first design of experiment cultivation experiment using *Ustilago maydis* MB215 (see Table A1 for experimental conditions). System Duetz®24-deep-well plate cultivations were performed with modified Tabuchi medium (MTM) containing 2-(N-morpholino) ethanesulfonic acid (MES) buffer and 4 g L^{-1} NH$_4$Cl at 30°C. Growth rate is averaged. Panel (b) shows experimental data with nine data points, which are arithmetic means from 5 to 8 measurements. Panel (c) shows the theoretical growth rate over glucose and acetate flux predicted by flux balance analysis (FBA). Nine points are simulated, of which one is not feasible, with linear interpolation between the points.

deteriorates the growth rate with increasing share of acetate (see Figure 1a). Due to the FBA findings, the acetate range was adapted during the performed experiments. The results in Figure 3a corrobo-rate previous findings that higher glucose concentrations result in lower growth rates (Liebal et al., 2022) and this sensitivity is

increased by higher acetate concentrations. Note that we interpolated linearly between the experimental data points to follow the concept of DoE and to make the results more visible to the reader and to improve the comparability with the FBA results. The co-feeding with 10 g L^{-1} acetate and 20 g L^{-1} glucose (#3 with ≈ 17% relative acetate C-mol ratio in Figure 3a) resulted in the highest observed growth rate of 0.066 h^{-1}. Additional data clarifying the relationship between substrate consumption rates and growth behavior of *U. maydis* is shown in Figure A1.

Figure A1a shows the comparison of glucose consumption to acetate consumption rate. In general, conditions with high glucose concentration had the highest substrate uptake rates for glucose and the lowest for acetate. The acetate consumption rate increases with increasing supplemented acetate concentration. However, the effect decreases as the supplemented glucose concentration increases. This indicates a diauxic growth behavior.

Considering Figure A1b, high glucose concentrations lead to high biomass production (condition 5–9). At the same time, conditions showed relatively low growth rates, which can be explained by the prolonged linear growth phases for those conditions (Table A1). On the other hand, conditions with lower glucose concentrations showed very high growth rates with low biomass formation.

Further, Figure A1b shows the comparison of nonspecific growth rate and corresponding cell-dry-weight (CDW) for the linear growth phase. As expected, higher glucose concentrations leads to higher biomass results because most of supplemented glucose can be used for biomass production.

The influence of acetate can be illustrated by comparing conditions 4 and 5 as the same concentration of glucose was used for both conditions. Nevertheless, the culture condition 4 with lower acetate concentration showed a significantly higher growth rate compared to condition 5. This was already observed during batch fermentations with *U. maydis* during previous experiments. The culture with supplemented acetate exhibited a lower growth rate with prolonged lag phase compared to *U. maydis* culture without acetate (Ullmann et al., 2021). Acetate does not seem to affect the biomass productivity since biomass is almost constant for all conditions with the same glucose concentration and variable acetate concentration.

To get further insights into how the metabolic configuration changes with respect to the feeding conditions, we measured the uptake rates that correspond to the nine co-feeding conditions (Figure 3b). There are three sets of measurements with increasing glucose and constant acetate concentrations (sets #2+#7, #1+#5+#9, #3+#8). All sets display a pronounced decrease in acetate uptake rate with a modest increase in glucose uptake rate. For example, for the measurements #1+#9, the glucose concentration increases from 10 to 80 g L^{-1}, the glucose uptake rate increases only from ≈0.45 to 0.9 mmol g$_{DW}^{-1}$ h^{-1}, while despite constant level, the acetate uptake decreases from ≈0.7 to below 0.2 mmol g$_{DW}^{-1}$ h^{-1}. The same effect is exerted by acetate on constant glucose levels: increasing the acetate concentration decreases glucose uptake rates (sets #2+#3, #4+#5+#6, #7+#8). In set #7+#8, whereas the glucose concentration

remains constant, the glucose uptake rate decreases from ≈1 to 0.2 mmol g$_{DW}^{-1}$ h^{-1} with an increase in acetate concentration from 2.5 to 10 g L^{-1}. Note the growth anomaly for the measurements #4, #7, and #9. Although the substrate uptake rates for glucose and acetate are comparable for the three measurements, the increase of acetate concentration causes a drop in the yield with conditions #7 and #9. Overall, the concentration growth profile in Figure 3a is reversed in the substrate uptake rate profile in Figure 3b. Measurements with high concentrations are mirrored to low uptake rates (e.g., #8) and vice versa (e.g., #2). Acetate causes weak acid stress and, hence, the cell responds with reduced uptake. At high glucose and acetate concentrations in the medium, substrate uptake is reduced. Maassen et al. (2014) showed that lower concentrations of glucose are likely to reduce osmotic stress, which has a positive effect on cellular growth.

The inhibiting effect of acetate on glucose consumption is absent in iUma22 for growth optimization. When comparing the experimental with the simulated growth rate in Figure 3c, the growth rates are overall in the same range. Especially, we find equivalent growth rates at low glucose and acetate fluxes (measurements #8 and #6). The results divert with increasing glucose and acetate flux. At conditions with high acetate flux, the experimental growth rate exceeds the simulated growth rate. One example for this is point #1, where the experimental growth rate is 0.046 h^{-1}, whereas the simulated growth rate is 0.03 h^{-1}. This low simulated growth rate is no outlier but following the trend lines of the simulation. The co-feeding conditions at point #3 do not furnish a feasible result, which matches the observations in Section 3.1.

3.4 | Itaconic acid production: Design of experiments and metabolic modeling enable finding the optimal co-feeding strategy

In a second DoE, for which we hypothesized combinatorial effects of cell growth, substrate uptake rates as well as itaconic acid production, nine different media combinations were tested (Table A2). The experimental DoE approach aims to gain a deeper understanding of how different combinations of the following factors, for example, glucose and sodium acetate, impact itaconic acid production. Itaconic acid production itself was evaluated by the responses titer and yield. Based on results shown in Section 3.1, FBA indicates that acetate improves the itaconic acid yield up to a share of 40% acetate on a carbon molar basis. Nevertheless, acetate is known to have the following effects on *U. maydis*. According to Kretschmer et al. (2018), acetate provokes mitochondrial stress in *U. maydis*. Higher concentrations of acetate not only cause acidification of the cytosol, leading to impaired enzyme activity, initiation of programmed cell death and increased levels of reactive oxygen species (ROS) but also reduce the expression of ROS detoxification mechanisms, boosting oxidative stress further. Due to the stated acetate toxicity, the acetate range was adapted during the performed DoE experiments despite the results obtained from FBA.

The DoE study returned the equation

$$\text{Ita-yield} = 6.58 \times 10^{-2} + 4.07 \times 10^{-3} \cdot c_{Ace} + 5.32 \times 10^{-4} \\ \cdot c_{Glc} \\ + 5.05 \times 10^{-5} \cdot c_{Glc} \cdot c_{Ace} - 4.36 \times 10^{-4} \\ \cdot c_{Ace}^2 - 2.62 \times 10^{-6} \cdot c_{Glc}^2, \tag{2}$$

for the calculation of itaconic acid yield from co-feeding conditions, where c_{Glc} and c_{Ace} are the concentrations of glucose and acetate, respectively. The equation uses the practically relevant substrate concentration as variable, and for comparison with the FBA a transformation of the concentrations into fluxes is necessary. For the transformation, we conducted an experimental study to correlate starting concentrations and uptake rates of glucose and acetate. The following linear regression models result in a coefficient of determination (R^2) 0.863 mmol g_{DW}^{-1} h^{-1} for v_{Glc} and 0.814 mmol g_{DW}^{-1} h^{-1} for v_{Ace}:

$$v_{Glc} = 0.97 - 9.22 \times 10^{-2} \cdot c_{Ace} + 3.16 \times 10^{-3} \\ \cdot c_{Glc} + 2.43 \times 10^{-4} \cdot c_{Glc} \cdot c_{Ace} \\ v_{Ace} = 0.3 + 6.87 \times 10^{-2} \cdot c_{Ace} - 2.5 \times 10^{-3} \cdot c_{Glc} \\ - 1.06 \times 10^{-2} \cdot c_{Glc} \cdot c_{Ace}, \tag{3}$$

where v are fluxes, c are the concentrations and Glc and Ace represent glucose and acetate, respectively. Note, that the glucose uptake flux is strongly and inversely controlled by the acetate concentration. The additional interaction term $c_{Glc} \cdot c_{Ace}$ displays the interactions between glucose and acetate concentrations. The correlation enables us to display the yield of itaconic acid over the glucose and acetate flux, which makes it comparable to the results from the FBA. In the FBA, we set a threshold on biomass, which is 50% of the maximal theoretical biomass flux at this point. We chose the threshold of 50% as a value between the typically assumed

minimal growth rate of 10% (see Figure A2a) and the parameterized growth rate of 93% (see Figure A2b). The parameterized growth rate furnishes the least error between the itaconic acid yield from the DoE and the FBA results when the error is defined as $0.5 \cdot (\text{yield}_{FBA} - \text{yield}_{DoE})^2$.

Figure 4 shows the results from the design of experiments study in Figure 4a,b and the results from the FBA in Figure 4c.

Note that in Figure 4a, we interpolated linearly between the experimental data points to follow the concept of DoE and to make the results more visible to the reader. The corresponding glucose concentration for Figure 4b,c ranges from 26 to 80 g L^{-1}, whereas the acetate concentration ranges from 1.5 to 11.5 g L^{-1}. This decreased concentration range is due to the conversion of concentration to flux. The functions for conversion are only available for a certain range of values (four of the nine data points could be used for the conversion). The FBA was conducted in steps of 1 g L^{-1} for glucose and 0.25 g L^{-1} for acetate, resulting in around 2200 FBA predictions in Figure 4c.

Figure 4a summarizes the results from the design of experiments study of the averaged itaconic acid yield obtained from varying acetate and glucose concentrations. The highest yield was obtained by high substrate concentrations. Thereby, glucose showed a higher impact on itaconic acid yield than a high acetate concentration. In Figure 4b, we observe the level of itaconic acid yield as a plateau without steep descends. More precisely, the yield of itaconic acid is 0.09 to 0.13 C-flux$_{Ita}$C-flux$_{C-sources}^{-1}$. The lowest yield corresponds to the highest acetate flux, whereas the highest yield is achieved when the acetate flux is low. From the FBA displayed in Figure 4c, we find that below a glucose flux level of around 0.3 mmol g_{DW}^{-1} h^{-1}, there is a descent. Below a glucose flux of around 0.2 mmol g_{DW}^{-1} h^{-1}, there is no feasible solution, which is in coherence with the observations in Section 3.1. Above a glucose flux of 0.4 mmol g_{DW}^{-1} h^{-1}, we find a plateau. The yield is predicted in the range of 0.12 to 0.70 C-flux$_{Ita}$C-flux$_{C-sources}^{-1}$. The lowest yield corresponds to the lowest glucose flux, whereas the highest yield is
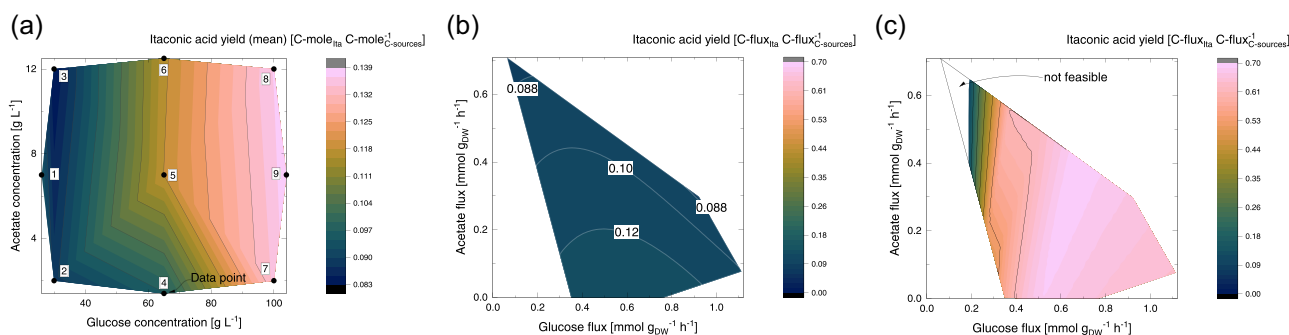

FIGURE 4 Itaconic acid yield depending on glucose and acetate concentration and uptake. The lines correspond to a constant yield. Panel (a) shows results from the design of experiments study of the averaged itaconic acid yield over acetate and glucose concentration (see Table A2 for experimental conditions). System Duetz®24-deep-well plate cultivations were performed with MTM containing CaCO3 buffer and 0.8 g L^{-1}NH4Cl at 30°C. Panel (b) shows results from the design of experiments study of itaconic acid yield over acetate and glucose flux (see also Table A2). Glucose flux and acetate flux were calculated from acetate and glucose concentrations via correlation in Equation (3), and itaconic acid yield was calculated via Equation (2). Panel (c) shows flux balance analysis (FBA) results of itaconic acid yield over acetate and glucose flux. Itaconic acid yield was calculated via FBA, with a threshold on biomass growth rate of 50% of the maximal theoretical biomass growth at each point.

observed in a medium region of around 0.5 to 0.7 mmol g_{DW}^{-1} h^{-1} glucose. Notably, the predicted yield of itaconic acid is higher than the experimental yield. The experimental yield is decreased by the formation of by-products in-vivo, unaccounted by the model. The results of the design of experiments analysis indicate that the itaconic acid yield is mainly dependent on the acetate uptake. In contrast, in the FBA, the glucose uptake appears to be decisive. One explanation for this phenomenon can be the toxicity of acetate to the microorganism. This toxicity is not included in FBA. Lastly, we observe a plateau with both methods, which indicates a coherence. Note that the discrepancy between model and experiment could be resolved by inclusion of experimental data in the model. Doing so, we would artificially adapt the simulation results to the experimental results, which, in our eyes, would not strengthen the significance of this study.

During DoE cultivation experiments with *U. maydis* MB215, the itaconic acid yield increased with increasing glucose concentration and for increasing acetate concentration when considering the equally high glucose concentrations. The maximum yield was reached with 0.14 ± 0.00 C-mol$_{Ita}$/C-mol$_{C-source}$ for the condition with the highest total amount of carbon with 100 g L^{-1} glucose and 12 g L^{-1} acetate. To get insights on the influence of glucose and acetate co-feeding on the itaconic acid yield compared to a standard glucose feed, cultivations with similar C-mol were performed for both (Figure 5).

For the cultivation, 90 g L^{-1} of glucose and 10 g L^{-1} of acetate were used. As these are no conditions used to create the DoE, the predictive power of this was tested at the same time. First, the

cultivation with glucose and acetate reached a yield of 0.15 ± 0.01 C-mol$_{Ita}$/C-mol$_{C-source}$. Compared with the DoE prediction 0.14 ± 0.01 C-mol$_{Ita}$/C-mol$_{C-source}$ the values do not differ significantly. The respective glucose reference cultivation reached a yield of 0.11 ± 0.00C-mol$_{Ita}$/C-mol$_{C-source}$ which is significantly lower compared to cultivation with acetate (Figure 5). Since the reached yield did not differ significantly from the model prediction, the validation was considered as successful, indicating that the model has an accurate predictive power regarding the yield for a defined substrate combination within the model ranges. Moreover, the comparison to a glucose reference with a similar total carbon amount showed that acetate has a positive effect on the itaconic acid production, which was already indicated in previous experiments Ullmann et al. (2021).

Further, an upscaling experiment in a controlled batch fermentation with 500 mL working volume was performed. Since itaconic acid is produced industrially in large bioreactors, this represents a comparable cultivation on laboratory scale. During batch fermentation, the dissolved oxygen (DO) level was monitored with an electrode and through varying stirring rates and gasflow the DO was kept at 80% over the cultivation duration based on previous studies (Hosseinpour Tehrani, Becker, et al., 2019, Hosseinpour Tehrani, Saur, et al., 2019). OD$_{600}$, maximum growth rate μ_{max}, carbon source consumption and itaconate production were monitored during cultivation for both tested conditions. For a test condition for upscaling experiments, 100 g L^{-1} glucose and 12 g L^{-1} acetate as well as a respective glucose reference were chosen, since the itaconic acid production was observed under this condition (yield) (Figure 6).

During batch fermentation, an itaconic acid production of 19.5 ± 5.0 g L^{-1} was observed for the acetate co-feeding condition (yield 0.17 ± 0.05 g g^{-1}). In contrast, sole glucose cultivation resulted in an itaconic acid yield of 0.12 ± 0.02 g g^{-1}. Calculating itaconic acid yield on a C-molar basis results in a yield of 0.21 ± 0.05 C-mol$_{Ita}$/C-mol$_{C-source}$ for acetate co-feeding and 0.17 ± 0.02 C-mol$_{Ita}$/C-mol$_{C-source}$ for glucose-only culture. The obtained results correspond to the itaconic acid production resulted in small scale proving a successful upscaling approach.

4 | CONCLUSION

FBA suggested that a carbon atom division of 40% for acetate and 60% for glucose achieves the highest itaconic acid yield. In the associated optimally simulated pathway, all AcCoA from acetate was used for citrate synthase and each glucose was converted to two malate, further fixing 2 mol CO_2 per glucose. This additional CO_2 fixation results into an increased yield on glucose. The strain optimization targeted high rates whereas the co-feeding flux simulation focused on high itaconic acid yields. The predictions center on glucose-related reactions for rate increases whereas the oxalacetic acid to malate reaction is a key reaction for high yields during co-feeding.
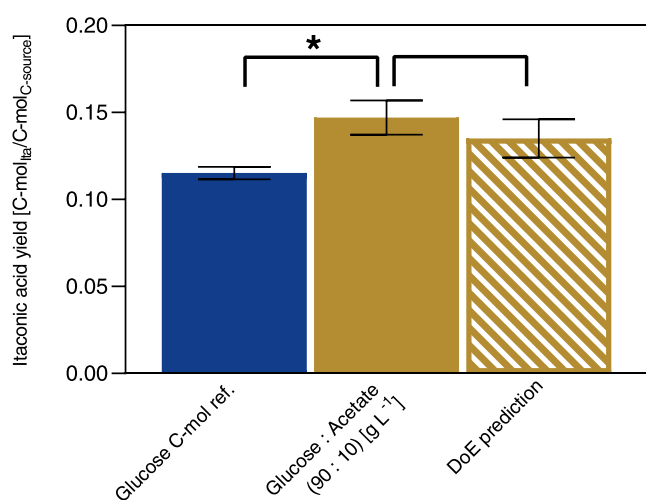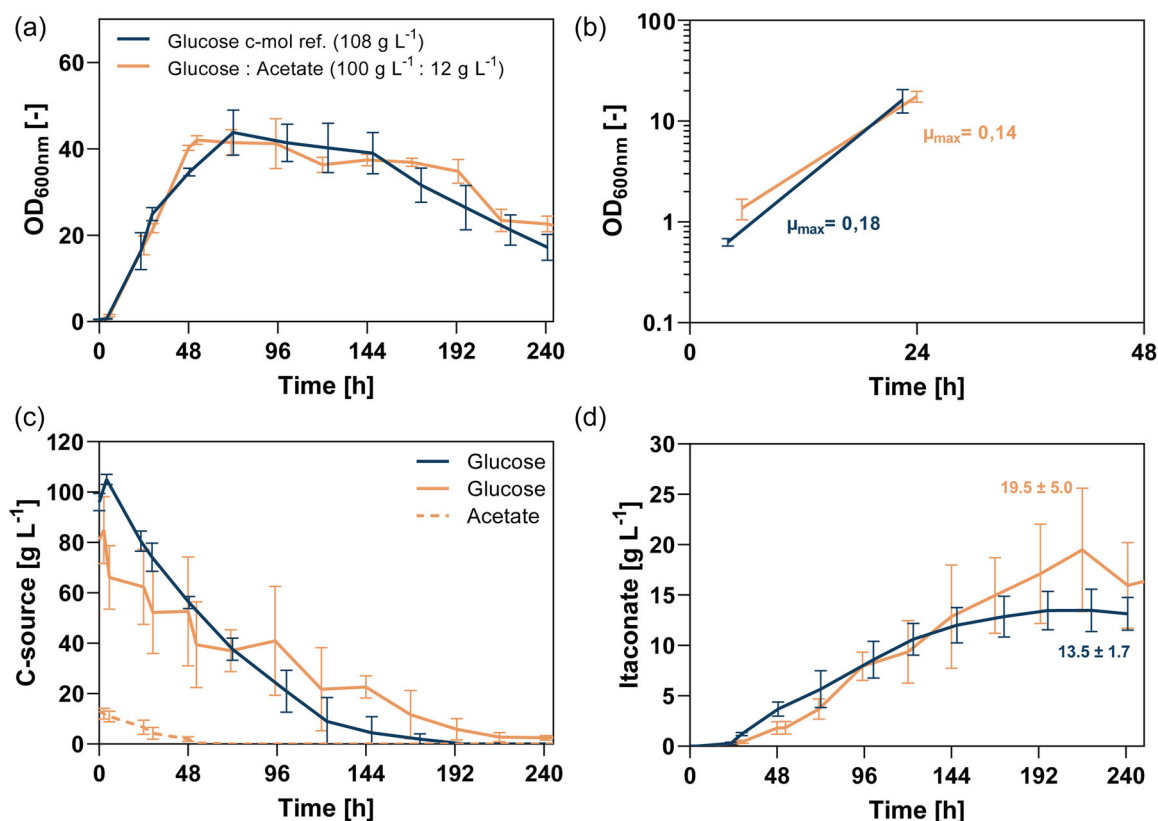

FIGURE 5 Comparison of itaconic acid yields for glucose and acetate co-feeding with standard glucose cultivation. The co-feeding of glucose and acetate (brown) was compared to the design of experiment prediction (shaded brown) and a glucose reference containing the same amount of total carbon (blue). System Duetz®24-deep-well plate cultivations were performed at 30°C with 0.8 g L^{-1} NH₄Cl and CaCO₃ buffer. Error bars indicate the deviation from the mean for n = 3. Statistically significant differences in itaconic acid production (0.01 < p < 0.05) are indicated as *.

FIGURE 6 Batch fermentation with 500 mL working volume. As carbon source, 100 g L^{-1} glucose and 12 g L^{-1} acetate as well as a respective glucose reference were chosen. Panel (a) shows the optical density (OD_{600}); (b) depicts the maximal growth rate μ_{max}. Panel (c) shows the depletion of the carbon source (C-source). Panel (d) shows the itaconic acid production.

Efficient co-feeding rests on a delicate balance between glucose and acetate consumption. The DoE data analysis shows a direct correlation of the itaconic acid yield with the acetate concentrations. However, because the substrates reciprocally inhibit their uptake rates, the rates will deteriorate with increasing concentrations. The simulation indicates a minimum uptake rate of glucose (0.5 mmol g_{DW}^{-1} h^{-1}) is necessary to profit from acetate. This is corroborated by the DoE, which displays highest acetate and yield robustness at a glucose uptake rate of 0.5 mmol g_{DW}^{-1} h^{-1}. This fragile substrate balance would have to be overcome for any successful industrial application by increasing robustness via mutations followed by a confirmation of the performance during large-scale cultivations. Also, fed-batch cultivations that keep the carbon source below detrimental concentrations will contribute to harvest the benefits of the CO_2-derived co-substrate acetate.

AUTHOR CONTRIBUTIONS

Anita L. Ziegler designed the computations (FBA and OptKnock) and carried out the project management. Lena Ullmann designed the laboratory experiments and the DoE studies. Manuel Boßmann performed the computations under the supervision of Anita L. Ziegler. Karla L. Stein performed the laboratory experiments under the supervision of Lena Ullmann. Ulf W. Liebal provided the updated metabolic network. Anita L. Ziegler, Lena Ullmann, and Ulf W. Liebal analyzed and discussed the data. Anita L. Ziegler, Lena Ullmann, Ulf W. Liebal, and Karla L. Stein wrote the manuscript draft. Alexander Mitsos and Lars M. Blank conceptualized the project, discussed the data and reviewed the draft. All authors read and approved the final manuscript.

ACKNOWLEDGMENTS

CONFLICT OF INTEREST STATEMENT

The authors declare no conflict of interest.

DATA AVAILABILITY STATEMENT

The updated genome-scale metabolic model iUma22 is available in our GitHub repository "Ustilago_maydis-GEM" as v1.1 at https://github.com/iAMB-RWTH-Aachen/Ustilago_maydis-GEM/tree/v1.1. The FBA and OptKnock computations underlying this article are

available in our GitHub repository "Ustilago_maydis-GEM" at https://github.com/iAMB-RWTH-Aachen/Ustilago_maydis-GEM/tree/master/data/AcetateCofeed.

ORCID

Anita L. Ziegler https://orcid.org/0000-0003-3502-6609

REFERENCES

Apaydin, M., Xu, L., Zeng, B., & Qian, X. (2017). Robust mutant strain design by pessimistic optimization. *BMC Genomics*, *18*(Suppl. 6), 677.

Becker, J., HosseinpourTehrani, H., Gauert, M., Mampel, J., Blank, L. M., & Wierckx, N. (2020). An *Ustilago maydis* chassis for itaconic acid production without by-products. *Microbial Biotechnology*, *13*(2), 350–362.

Becker, J., Liebal, U. W., Phan, A. N., Ullmann, L., & Blank, L. M. (2023). Renewable carbon sources to biochemicals and fuels: Contributions of the smut fungi Ustilaginaceae. *Current Opinion in Biotechnology*, *79*, 102849.

Burgard, A. P., Pharkya, P., & Maranas, C. D. (2003). Optknock: A bilevel programming framework for identifying gene knockout strategies for microbial strain optimization. *Biotechnology and Bioengineering*, *84*(6), 647–657.

Djelassi, H., & Mitsos, A. (2019). *libale—a library for algebraic-logical expression trees*. https://git.rwth-aachen.de/avt.svt/public/libale.git

Duetz, W. A., Rüedi, L., Hermann, R., O'Connor, K., Büchs, J., & Witholt, B. (2000). Methods for intense aeration, growth, storage, and replication of bacterial strains in microtiter plates. *Applied and Environmental Microbiology*, *66*(6), 2641–2646.

Ebrahim, A., Lerman, J. A., Palsson, B. O., & Hyduke, D. R. (2013). Cobrapy: Constraints-based reconstruction and analysis for Python. *BMC Systems Biology*, *7*, 74.

Enjalbert, B., Millard, P., Dinclaux, M., Portais, J. -C., & Létisse, F. (2017). Acetate fluxes in *Escherichia coli* are determined by the thermodynamic control of the Pta-AckA pathway. *Scientific Reports*, *7*, 42135.

Geiser, E., Ludwig, F., Zambanini, T., Wierckx, N., & Blank, L. M. (2016). Draft genome sequences of itaconate-producing Ustilaginaceae. *Genome Announcements*, *4*(6), e01291-16.

Geiser, E., Przybilla, S. K., Engel, M., Kleineberg, W., Büttner, L., Sarikaya, E., Hartog, T. d., Klankermayer, J., Leitner, W., Bölker, M., Blank, L. M., & Wierckx, N. (2016). Genetic and biochemical insights into the itaconate pathway of *Ustilago maydis* enable enhanced production. *Metabolic Engineering*, *38*, 427–435.

Geiser, E., Wiebach, V., Wierckx, N., & Blank, L. M. (2014). Prospecting the biodiversity of the fungal family Ustilaginaceae for the production of value-added chemicals. *Fungal Biology and Biotechnology*, *1*, 2.

Gurobi Optimization, LLC. (2022). *Gurobi optimizer reference manual*. https://www.gurobi.com

Gyamerah, M. (1995). Factors affecting the growth form of *Aspergillus terreus* NRRL 1960 in relation to itaconic acid fermentation. *Applied Microbiology and Biotechnology*, *44*(3–4), 356–361.

Hosseinpour Tehrani, H., Becker, J., Bator, I., Saur, K., Meyer, S., RodriguesLóia, A. C., Blank, L. M., & Wierckx, N. (2019). Integrated strain- and process design enable production of 220 g l-1 itaconic acid with *Ustilago maydis*. *Biotechnology for Biofuels*, *12*, 263.

Hosseinpour Tehrani, H., Saur, K., Tharmasothirajan, A., Blank, L. M., & Wierckx, N. (2019). Process engineering of pH tolerant ustilago cynodontis for efficient itaconic acid production. *Microbial Cell Factories*, *18*(1), 213.

Hosseinpour Tehrani, H., Tharmasothirajan, A., Track, E., Blank, L. M., & Wierckx, N. (2019). Engineering the morphology and metabolism of pH tolerant ustilago cynodontis for efficient itaconic acid production. *Metabolic Engineering*, *54*, 293–300.

Jungen, D., Zingler, A., Djelassi, H., & Mitsos, A. (2023). *libdips—A library for discretization-based semi-infinite programming solvers*. https://git.rwth-aachen.de/avt-svt/public/libdips/

Kämper, J., Kahmann, R., Bölker, M., Ma, L. -J., Brefort, T., Saville, B. J., Banuett, F., Kronstad, J. W., Gold, S. E., Müller, O., Perlin, M. H., Wösten, H. A. B., de Vries, R., Ruiz-Herrera, J., Reynaga-Peña, C. G., Snetselaar, K., McCann, M., Pérez-Martín, J., Feldbrügge, M., Basse, C. W., Steinberg, G., Ibeas, J. I., Holloman, W., Guzman, P., Farman, M., Stajich, J. E., Sentandreu, R., González-Prieto, J. M., Kennell, J. C., Molina, L., Schirawski, J., Mendoza-Mendoza, A., Greilinger, D., Münch, K., Rössel, N., Scherer, M., Vranes, M., Ladendorf, O., Vincon, V., Fuchs, U., Sandrock, B., Meng, S., Ho, E. C. H., Cahill, M. J., Boyce, K. J., Klose, J., Klosterman, S. J., Deelstra, H. J., Ortiz-Castellanos, L., Li, W., Sanchez-Alonso, P., Schreier, P. H., Häuser-Hahn, I., Vaupel, M., Koopmann, E., Friedrich, G., Voss, H., Schlüter, T., Margolis, J., Platt, D., Swimmer, C., Gnirke, A., Chen, F., Vysotskaia, V., Mannhaupt, G., Güldener, U., Münsterkötter, M., Haase, D., Oesterheld, M., Mewes, H. -W., Mauceli, E. W., DeCaprio, D., Wade, C. M., Butler, J., Young, S., Jaffe, D. B., Calvo, S., Nusbaum, C., Galagan, J., & Birren, B. W. (2006). Insights from the genome of the biotrophic fungal plant pathogen *Ustilago maydis*. *Nature*, *444*(7115), 97–101.

Karaffa, L., Díaz, R., Papp, B., Fekete, E., Sándor, E., & Kubicek, C. P. (2015). A deficiency of manganese ions in the presence of high sugar concentrations is the critical parameter for achieving high yields of itaconic acid by *Aspergillus terreus*. *Applied Microbiology and Biotechnology*, *99*(19), 7937–7944.

Kim, J., Reed, J. L., & Maravelias, C. T. (2011). Large-scale bi-level strain design approaches and mixed-integer programming solution techniques. *PLoS one*, *6*(9), e24162.

Kretschmer, M., Lambie, S., Croll, D., & Kronstad, J. W. (2018). Acetate provokes mitochondrial stress and cell death in *Ustilago maydis*. *Molecular Microbiology*, *107*(4), 488–507.

Kuenz, A., & Krull, S. (2018). Biotechnological production of itaconic acid-things you have to know. *Applied Microbiology and Biotechnology*, *102*(9), 3901–3914.

Liebal, U. W., Ullmann, L., Lieven, C., Kohl, P., Wibberg, D., Zambanini, T., & Blank, L. M. (2022). *Ustilago maydis* metabolic characterization and growth quantification with a genome-scale metabolic model. *Journal of Fungi*, *8*(5), 524.

Maassen, N., Panakova, M., Wierckx, N., Geiser, E., Zimmermann, M., Bölker, M., Klinner, U., & Blank, L. M. (2014). Influence of carbon and nitrogen concentration on itaconic acid production by the smut fungus *Ustilago maydis*. *Engineering in Life Sciences*, *14*(2), 129–134.

Martínez-Espinoza, A. D., García-Pedrajas, M. D., & Gold, S. E. (2002). The Ustilaginales as plant pests and model systems. *Fungal Genetics and Biology*, *35*(1), 1–20.

Okabe, M., Lies, D., Kanamasa, S., & Park, E. Y. (2009). Biotechnological production of itaconic acid and its biosynthesis in *Aspergillus terreus*. *Applied Microbiology and Biotechnology*, *84*(4), 597–606.

Orth, J. D., Thiele, I., & Palsson, B. Ø. (2010). What is flux balance analysis? *Nature Biotechnology*, *28*(3), 245–248.

Park, J. O., Liu, N., Holinski, K. M., Emerson, D. F., Qiao, K., Woolston, B. M., Xu, J., Lazar, Z., Islam, M. A., Vidoudez, C., Girguis, P. R., & Stephanopoulos, G. (2019). Synergistic substrate cofeeding stimulates reductive metabolism. *Nature Metabolism*, *1*(6), 643–651.

Ren, S., Zeng, B., & Qian, X. (2013). Adaptive bi-level programming for optimal gene knockouts for targeted overproduction under phenotypic constraints. *BMC Bioinformatics*, *14* (Suppl. 2), S17.

Roe, A. J., McLaggan, D., Davidson, I., O'Byrne, C., & Booth, I. R. (1998). Perturbation of anion balance during inhibition of growth of *Escherichia coli* by weak acids. *Journal of Bacteriology*, *180*(4), 767–772.

Romero-Aguilar, L., Hernández-Morfín, K. D., Guerra-Sánchez, G., & Pardo, J. P. (2023). Metabolic changes and antioxidant response in *Ustilago maydis* grown in acetate. *Journal of Fungi (Basel, Switzerland)*, *9*(7), 749.

Russell, J. B., & Diez-Gonzalez, F. (1998). The effects of fermentation acids on bacterial growth. *Advances in Microbial Physiology*, *39*, 205–234.

Saha, B. C. (2017). Emerging biotechnologies for production of itaconic acid and its applications as a platform chemical. *Journal of Industrial Microbiology & Biotechnology*, *44*(2), 303–315.

Schellenberger, J., Que, R., Fleming, R. M. T., Thiele, I., Orth, J. D., Feist, A. M., Zielinski, D. C., Bordbar, A., Lewis, N. E., Rahmanian, S., Kang, J., Hyduke, D. R., & Palsson, B. Ø. (2011). Quantitative prediction of cellular metabolism with constraint-based models: The COBRA Toolbox v2.0. *Nature Protocols*, *6*(9), 1290–1307.

Schipper, K. (2009). *Charakterisierung eines* Ustilago maydis *genclusters, das für drei neuartige sekretierte effektoren kodiert*. Philipps-Universität Marburg.

Steiger, M. G., Wierckx, N., Blank, L. M., Mattanovich, D., & Sauer, M. (2017). *Itaconic acid—An emerging building block*. Industrial Biotechnology.

Tepper, N., & Shlomi, T. (2010). Predicting metabolic engineering knockout strategies for chemical production: Accounting for competing pathways. *Bioinformatics*, *26*(4), 536–543.

Ullmann, L., Phan, A. N. T., Kaplan, D. K. P., & Blank, L. M. (2021). Ustilaginaceae biocatalyst for co-metabolism of CO_2-derived substrates toward carbon-neutral itaconate production. *Journal of Fungi*, *7*(2), 98.

Ullmann, L., Wibberg, D., Busche, T., Rückert, C., Müsgens, A., Kalinowski, J., & Blank, L. M. (2022). Seventeen Ustilaginaceae high-quality genome sequences allow phylogenomic analysis and provide insights into secondary metabolite synthesis. *Journal of Fungi*, *8*(3), 269.

Varma, A., & Palsson, B. O. (1994). Stoichiometric flux balance models quantitatively predict growth and metabolic by-product secretion in wild-type *Escherichia coli* w3110. *Applied and Environmental Microbiology*, *60*(10), 3724–3731.

Wege, S.-M., Gejer, K., Becker, F., Bölker, M., Freitag, J., & Sandrock, B. (2021). Versatile CRISPR/Cas9 systems for genome editing in *Ustilago maydis*. *Journal of fungi*, *7*(2), 149.

APPENDIX A

TABLE A1 Experimental conditions for first design of experiments approach.

Condition no.	Replicates	Glucose (g L⁻¹)	Acetate (g L⁻¹)
1	5	9.6	6.25
2	5	20.0	2.5
3	5	20.0	10.0
4	5	45.0	0.9
5	8	45.0	6.25
6	5	45.0	11.5
7	5	70.0	2.5
8	5	70.0	10
9	5	80.3	6.25

Note: Conditions to be tested were generated with the software design expert. Cultivations were performed in system Duetz®24 deep-well microtiter plates at 30°C using modified Tabuchi medium with 2-(N-morpholino) ethanesulfonic acid buffer and $4\,gL^{-1}$ NHCl.

TABLE A2 Experimental conditions for second design of experiments approach.

Condition no.	Replicates	Glucose (g L⁻¹)	Acetate (g L⁻¹)
1	2	26	7
2	3	30	2
3	3	30	12
4	2	65	1.4
5	8	65	7
6	2	65	12.5
7	3	100	2
8	3	100	12
9	2	104	7

Note: Conditions to be tested were generated with the software Design Expert. Cultivations were performed in System Duetz®24 deep-well microtiter plates at 30°C using MTM with $CaCO_3$ buffer and $0.8\,gL^{-1}$ NH_4Cl.
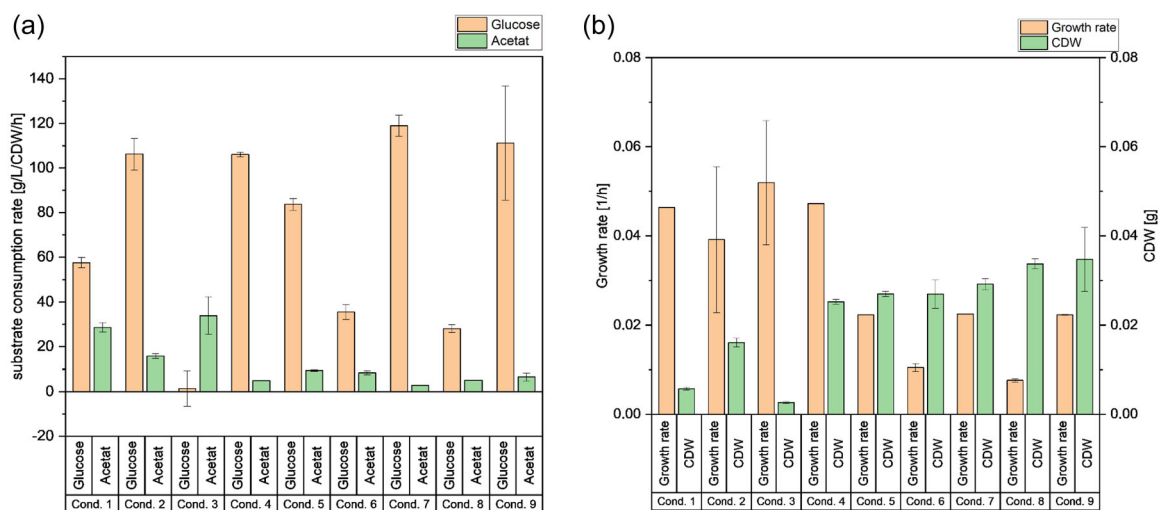
FIGURE A1 Experimental results for the first Design of Experiments study (experimental conditions see Table A1). Panel (a) shows the glucose and acetate consumption. Panel (b) shows the comparison of cell dry weight and growth rates.
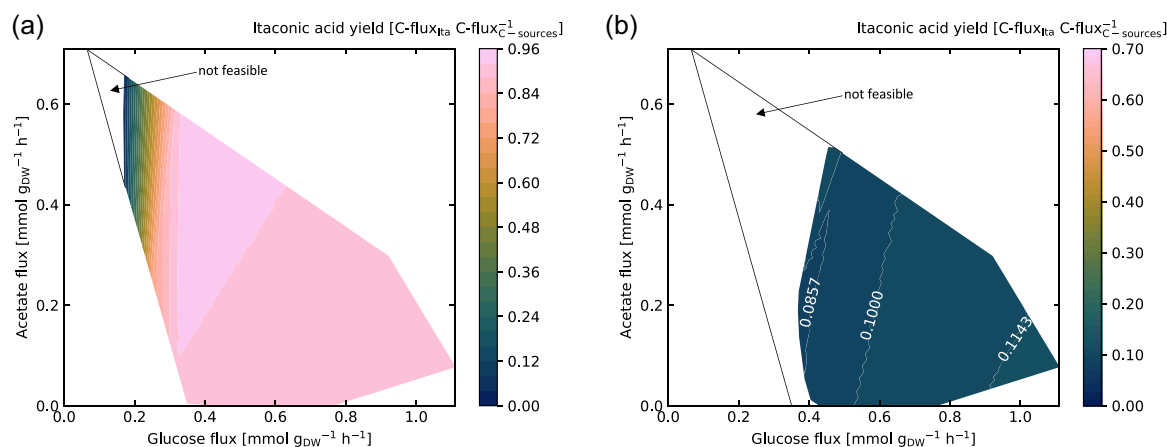

FIGURE A2 Itaconic acid yield depending on glucose and acetate uptake. Flux balance analysis (FBA) results of itaconic acid yield over acetate and glucose flux. Itaconic acid yield was calculated via FBA, with a threshold on biomass growth rate of 10% (a) and of 93% (b) of the maximal theoretical biomass growth at each point.